Electronic Supplementary Information

One-Step Synthesis of Fe-Au Core-Shell Magnetic-Plasmonic Nanoparticles Driven by Interface Energy Minimization

Anna Tymoczko,[1] Marius Kamp,[2] Christoph Rehbock,[1] Lorenz Kienle,[2] Elti Cattaruzza,[3] Stephan Barcikowski[1,] and Vincenzo Amendola[4,*]*

[1] Technical Chemistry I and Center for Nanointegration Duisburg-Essen (CENIDE), University Duisburg-Essen, Universitätstr. 7, 45141 Essen, Germany
[2] Faculty of Engineering CAU Kiel, Institute for Materials Science, Synthesis and Real Structure, Kaiserstraße 2, 24143 Kiel, Germany
[3] Department of Molecular Sciences and Nanosystems, Università Ca' Foscari Venezia, via Torino 155/b, I-30172 Venezia-Mestre, Italy
[4] Department of Chemical Sciences, University of Padova, via Marzolo 1, I-35131 Padova, Italy
* stephan.barcikowski@uni-due.de, vincenzo.amendola@unipd.it

Materials and methods.

S1. Thin film preparation.

Fe-Au films were prepared at room temperature by radiofrequency magnetron multitarget sputtering deposition of iron and gold, in pure Ar atmosphere at a working pressure of 40×10^{-4} mbar. Two different 13.56 MHz radiofrequency sources were used for iron and gold, respectively. Substrates were sodalime glass slides cleaned according to a previously published procedure.[1] Before deposition, the soda-lime substrates were rf-biased at 20 W for 20 min, to remove possible surface contaminants (removed layer thickness around 10 nm). During deposition, the sample holder was rotating at 10 Hz. The rf power to the 2 in. diameter targets was 40 W for iron and 20 W for gold. Different deposition times were used to obtain layers of the prescribed thickness. The final thickness of the different layers was measured by Rutherford backscattering spectrometry (RBS) by using a 2.2 MeV $4He^+$ beam.[2] The incident direction was normal to the sample surface, and scattered particles were detected at the angle of 160°. For each deposition, different RBS measurements were performed in randomly selected film points. Film thickness was calculated by using the density value of the bulk phases. Relative random uncertainty on film thickness was less than 2% in all films.

Film thickness and corresponding Fe:Au ratios are reported in Table S1 below:

Table S1. Film thickness

Film type	Thickness	Fe:Au ratio
Au+Fe/glass	76 nm	0.90
Fe/Au/glass	32 nm / 45 nm	1.03
Au/Fe/Au/Fe/glass	21 nm / 17 nm / 22 nm / 17 nm	1.13
Au/Fe/glass	43 nm / 33 nm	1.10

S2. Laser ablation synthesis.

LASiS was performed in Acetone (HPLC Plus, >99.9%, Sigma-Aldrich) adapting a previously described procedure,[3] with either 6 ns, 1064 nm pulses of a Nd:YAG laser with pulse energy of 22.6 mJ and fluence of 3.1 J/cm^2, or 10 ps, 1064 nm pulses of a Nd:YAG laser with pulse energy of 0.08 mJ and fluence of 4 J/cm^2. The film targets were placed in acetone at the bottom of the glassy batch-chamber, and ablated from the top. The focal point was moved at each laser pulse in order to ablate a different point of the film at each single laser pulse, with a minimum distance of 0.2 mm between each ablation crater.

Coating with NTP was performed in two steps: first, the thiol was added to the NPs dispersion in acetone with a final concentration of 10^{-3} M, then the NPs were attracted with a permanent NdFeB magnet at the bottom of the vial, the supernatant removed, and fresh liquid solution added again. The latter procedure was repeated 7 times. Finally, NPs were redispersed by ultrasounds and drop casted on a soda-lime microscope slide embedded between two permanent NdFeB magnets to obtain NPs alignment during liquid evaporation.

S3. Analysis of nanoparticles.

UV−vis spectroscopy of nanoparticle colloidal suspension in acetone was performed using a Cary 5 UV−vis−NIR spectrophotometer in 1 cm quartz cuvettes. Stability of the laser synthesized colloids was also assessed by UV-vis spectroscopy, by monitoring absorbance over time (an example is reported in Figure S1 below).

In experiments of Figures 2B-C, Raman spectra were collected with a 50X microscope objective of a DXR ThermoScientific microRaman equipped with a 532 nm laser. NPs were deposed on a microscope slide embedded between two permanent NdFeB magnets, as described above. MG solutions (10000, 500, 200, 100, 50 and 10 nM) were drop casted (1000 nL each drop) onto NPs spots before collection of Raman spectra.

For experiments of Figure 2E, a 10X objective and a piezo stage were used for collecting bidimensional Raman maps on the areas delimitated by the red square in the optical microscope images shown in the same Figure. The maps were collected on an area of 1500 x 1600 μm^2 at 532 nm with acquisition time of 30 s for each point and a power of 1.5 mW. Maps of Figure 2E refer to the Raman spectrum intensity at 1615 cm^{-1}. For accumulation of CS NPs, a cylindrical NdFeB permanent magnet (2 mm in diameter for 8 mm length) was placed below the glass substrate before drop casting of the aqueous solution. Colloid concentration is indicated in the main text. For this experiment, CS NPs were obtained in the following way: the colloid as obtained from LASiS was placed in a glass vial on top of a 40 mm x 40 mm NdFeB permanent magnet; after 3 h acetone was completely removed with a micropipette and replaced with distilled water, and NPs were redispersed by ultrasounds. As a reference, commercial citrate stabilized 50 nm Au NPs were used (Sigma Aldrich) at a final concentration of 22 μg/mL.

The size and the internal composition of laser-generated NPs were determined using transmission electron microscopy (FEI Tecnai F30 STWIN G) in STEM HAADF or EDS modality. 10 μL of each colloid dispersion were pipetted onto a carbon-coated copper microgrid and dried overnight. The Feret diameter of the sample was measured for a minimum of 500 NPs for each sample with help of Image J software.

S4. Numerical calculations.

G_{SERS} was evaluated as the 4th power of the ratio between the local electric field E_{loc} in the proximity to the surface of the metal nanostructure and the incident electric field E_0 from a linearly polarized 532 nm electromagnetic radiation, according to ref. [4–6]. E_{loc} was calculated by the discrete dipole approximation (DDA) method using the DDSCAT 7.1 and the relative DDFIELD packages.[7] The Fe-Au CS dimer of Figure 2D was built with two spheres of, respectively, 70 and 62 nm in external diameter and 52 and 46 nm in core diameter, with an interparticle gap of 2 nm. The final target resulted in 6.5 10^5 dipoles and interdipole spacing lower than 1 nm. The Fe-Au CS dimer of Figure S4A was built with two equal spheres of 22.4 nm in external diameter (according to the average NPs diameter extracted from the size histogram of Figure 1F) and 4.4 nm in shell thickness (according to the average NPs shell thickness extracted from the histogram in Figure S4B), and with an interparticle gap of 1 nm. The final target resulted in 7.6 10^5 dipoles and interdipole spacing lower than 1 nm. For metal particles in the 2–200 nm size range, an error smaller than 10% is achieved using a number of dipoles at least of the order of 10^4 and using an interdipole spacing much smaller than the wavelength of interest,[7–9] as in the present case. The optical constants of Au and Fe were obtained from ref.[10] and [11] respectively. The optical constants were corrected for the particle size, as reported previously.[6,12]

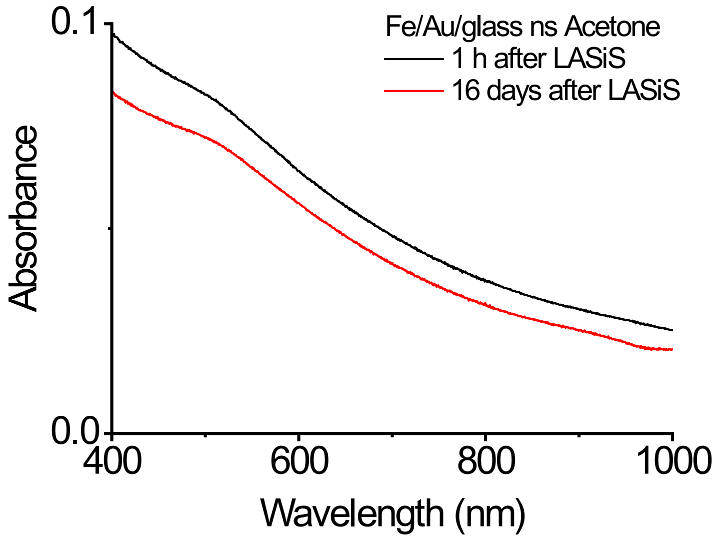

Figure S1. UV-vis spectra of the colloid obtained by ns LASiS with the Fe/Au/glass film in acetone, collected 1 h (black line) and 16 days (red line) after the synthesis. A limited decrease in absorbance is observed after 16 days, that is still the 87 ± 1 % of its value 1h after LASiS.

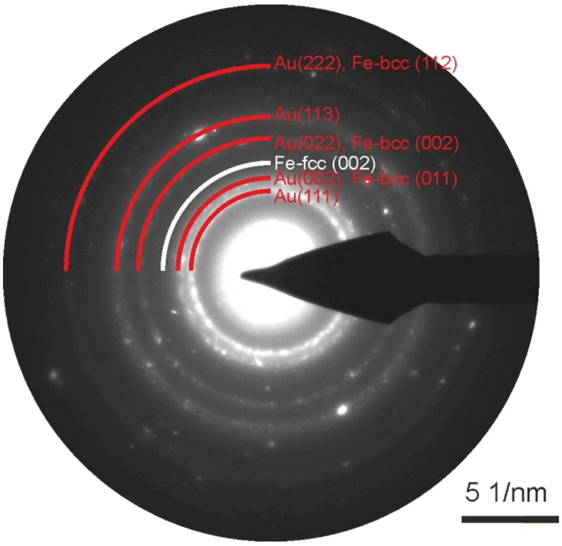

Figure S2. SAED pattern of Fe-Au CS NPs synthesized from alloy target. The intensity is distributed on concentric rings, which coincides with the intensities of Au-fcc and Fe-bcc phase (the respective lattice planes are indicated in red). By superimposing of the lattice spacing (Au-fcc and Fe-bcc) a direct assignment to the Fe-bcc phase is not possible, except when all further phases of Fe can be precluded. The only additional known stable metal iron phase is Fe-fcc. However, the position of the Fe-fcc (002) reflection (marked in white) shows no intensity in the experiment, confirming the absence of this phase.

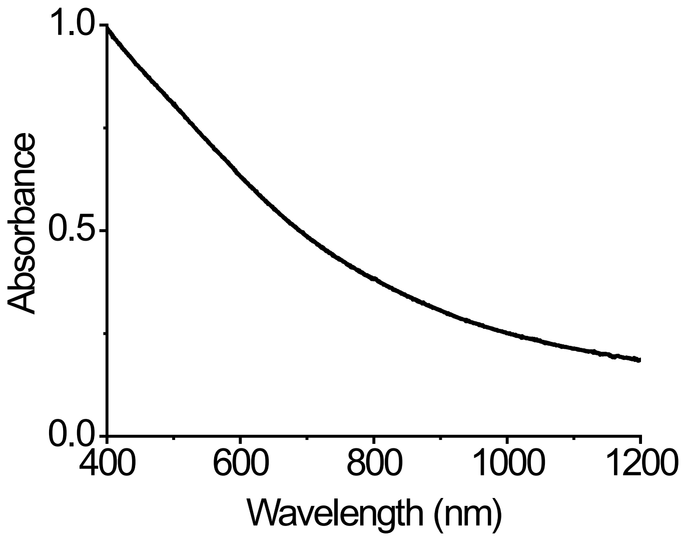

Figure S3. UV-vis absorption spectrum of the NPs in acetone.

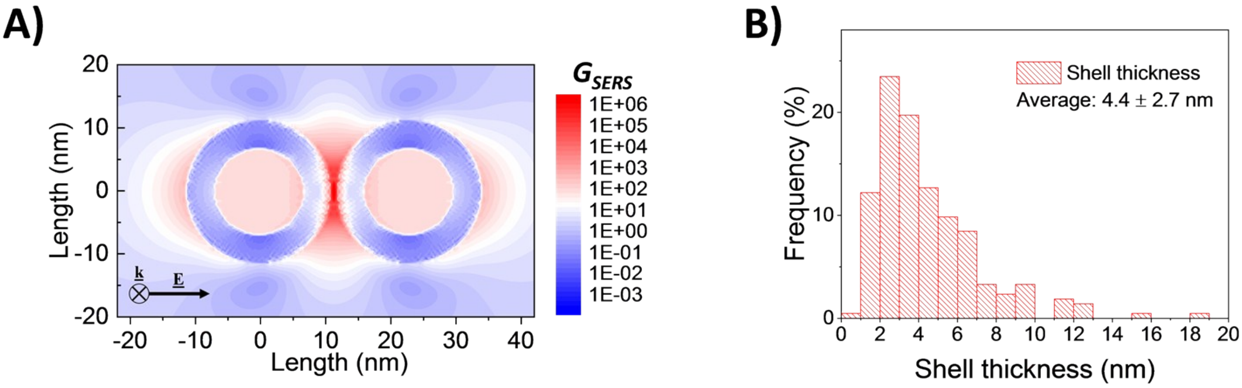

Figure S4. A) Bidimensional map of SERS enhancement factor (G_{SERS}) for 532 nm excitation, calculated for a dimer of CS NPs with average size of 22.4 nm (according to the size histogram reported in Figure 1F) and shell thickness of 4.4 nm (according to the TEM measured histogram of shell thickness reported in Figure S3B).

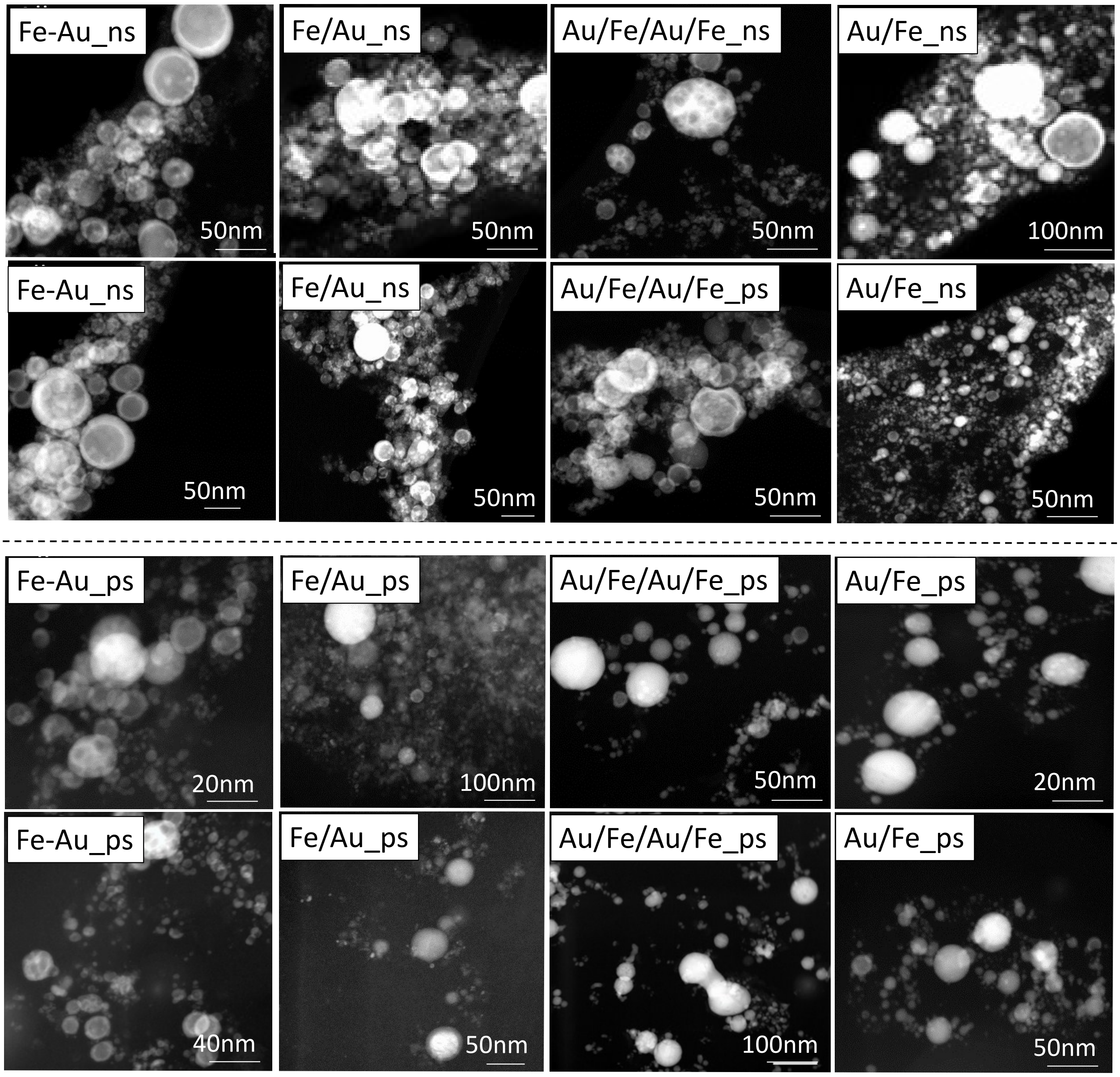

Figure S5. Representative STEM-HAADF pictures for all samples.

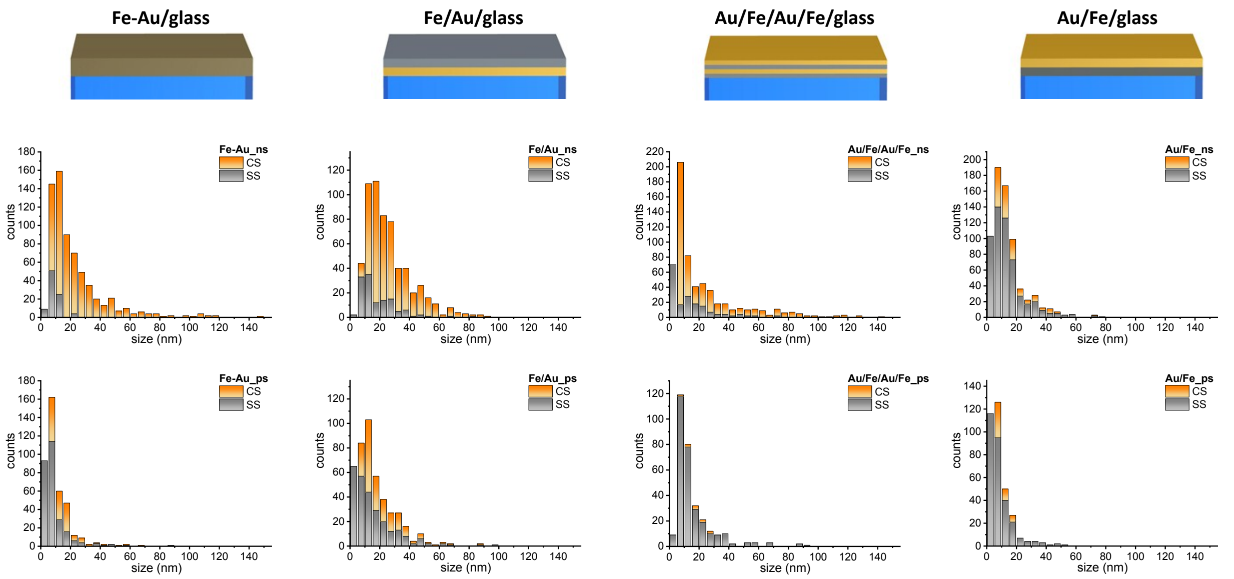

Figure S6. Cumulative histogram (CS+SS counts) showing number-weighted particle diameter distribution for all synthetized Fe-Au colloids.

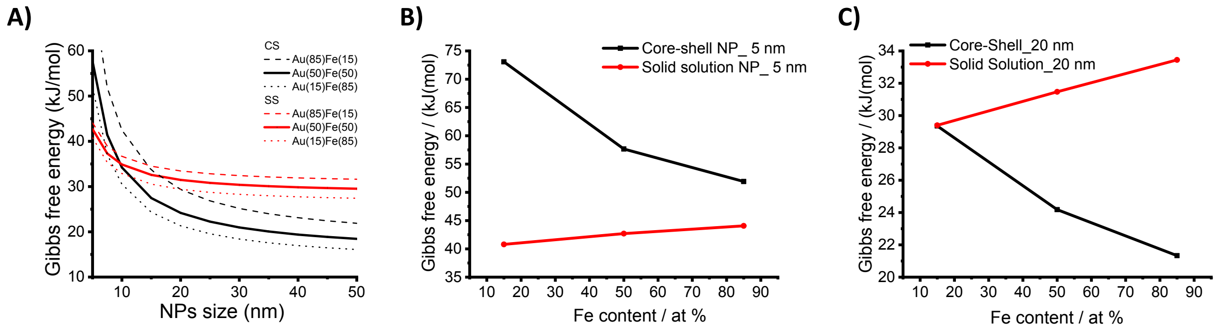

Figure S7. (A) Plot of Gibbs free energy calculated for SS (red lines) and CS (black lines) as a function of NPs size, and for three representative compositions: Fe(15)Au(85) (dashed lines), Fe(50)Au(50) (continuous lines), and Fe(85)Au(15) (dotted lines). (B-C) Plot of Gibbs free energy for CS (black dots) and SS (red dots) for the three compositions, for nanospheres with size of 5 nm (B) and 20 nm (C).

S5. Thermodynamic model for Gibbs free energy in SS and CS NPs.

The Gibbs free energy (G) was separately calculated for solid solution (SS) and core-shell (CS) nanoparticles. In the SS there is a homogeneous distribution of both elements within the particle, while the CS is composed by an iron core covered by a gold shell. Besides, the thermodynamic model only considers spherical particles with no faceting involved, therefore average surface energy values can be used, namely differences in interface/surface energies for different facets are ignored. It is also assumed that there is no stress at the interface, according to analogous studies reported in literaure.[13,14] Finally, interactions with the solvent are not considered in this model.

1. Model for calculation of the Gibbs free energy for SS NPs (G_{SS})

$\mathbf{G_{ss} = X_{Au}G_{Au} + X_{Fe}G_{Fe} + \Delta G_{mix} + (2\gamma_{ss}V_{AuFe})/(D/2)}$ *(eq. S1)*

with

D: the diameter of the particle

$\mathbf{X_{Fe}}$, $\mathbf{X_{Au}}$: the mole fraction of Au and Fe respectively

$\mathbf{G_{Au}}$, $\mathbf{G_{Fe}}$: the molar free energies of pure Au (G_{Au} = -14.1kJ/mol) and Fe (G_{Fe} = -7.95 kJ/mol)[15]

$\mathbf{\Delta G_{mix}} = \Delta H_{mix} - T\Delta S_{mix}$: the excess free energy of the alloy phase due to mixing (ΔG_{mix} = 39.296 kJ/ mol)[16]

$\boldsymbol{\gamma_{ss}}$: the size dependent specific surface energy (surface energy per unit area) of the nanoparticle with solid solution of Au and Fe atoms, given by

$\gamma_{ss} = N\,E_s(D) / \pi\alpha N_A D^2$ [Jm^{-2}] *(eq. S2)*

with

N : the number of atoms on the surface of a particle of diameter **D** with fcc solid solution structure, that is

$\mathbf{N} = \pi\alpha f^{-2/3} n^{2/3}$

with

α : the shape factor (defined as the surface area ratio of non-spherical and spherical nanoparticles of identical volumes); α = 1 for spherical nanoparticles[16]

f : the packing fraction for different structures; 0.74 was used for fcc cell

n : total number of atoms in the particle

with

$\mathbf{n} = R^3/r^3$

R = D/2 : the radius of the nanoparticle

r : the composition weighted average of $\mathbf{r_{Au}}$ and $\mathbf{r_{Fe}}$, the atomic radii of the elements in the fcc cell, given by

r_{Au} : 0.288 nm (for fcc structure)[17]

r_{Fe} : 0.258 nm (for fcc structure)[18]

$E_s(D)$: the size-dependent specific surface energy for a particle, given by[13,19]

$E_s(D)$ $= \{2-[Z_s(D)/Z_b] -[Z_s(D)/Z_b]^{1/2}\}E_{ci}(D)/2$

with

$E_{ci}(D)$ $= E_c(D)/\{1-p(D)\{2-[Z_s[D]/Z_b]- -[Z_s[D]/Z_b]^{1/2}\}/2$

where:

$p(D)$ $= N_s(D)/N_{tot}(D)$: the relation between the total number of atoms present on the surface, **$N_s(D)$**, and inside a particle, **$N_{tot}(D)$**, of a given size, respectively

$Z_s(D)$: size dependent average coordination number of surface atoms

Z_b : average coordination number of the internal atoms

$E_c(D)$: size and composition dependent cohesive energy, given by

$E_c(D)$ $= x_{Au}E_{Au}\ (1-(\alpha D^2/nd_{Au}^2) + x_{Fe}E_{Fe}\ (1-(\alpha D^2/nd_{Fe}^2) - X_{Au}X_{Fe}\ A$

X_{Au} , X_{Fe} : the molar fraction of Au and Fe, respectively

E_{Au} , E_{Fe} : the bulk cohesive energies of Au and Fe, respectively

E_{Au} = 368 kJ/mol[20]

E_{Fe} = 413 kJ/mol[16]

d_{Au} , d_{Fe} : the atomic diameters of Au and Fe, respectively

n : the total number of atoms in the particle

A : interaction parameter with a value of 60 kJ/mol[16]

N_A : Avogadro's number

and resulting in:

Table S2. The size dependent specific surface energy (surface energy per unit area) of the Au-Fe solid solution nanoparticle for three representative compositions

	$\gamma_{ss}(d_{Au},d_{Fe})$ (J/m^{-2})		
NPs size / nm	**$Au_{15}Fe_{85}$**	**$Au_{50}Fe_{50}$**	**$Au_{85}Fe_{15}$**
5	2.1	2.09	1.88
7.5	2	1.96	1.77
10	2	1.91	1.72
15	1.99	1.87	1.69
20	1.98	1.85	1.67
25	1.97	1.84	1.66
30	1.96	1.83	1.65
35	1.96	1.83	1.65
40	1.95	1.83	1.65

45	1.95	1.82	1.65
50	1.95	1.82	1.65
60	1.95	1.82	1.65
70	1.95	1.82	1.65
120	1.95	1.82	1.65
170	1.95	1.82	1.65

$\mathbf{V_{AuFe}}$: the molar volume of fcc AuFe solid solution, with

$\mathbf{V_{AuFe}} = X_{Au} \cdot V_{Au} + X_{Fe} \cdot V_{Fe}$

Calculated and summarized in Table S3:

Table S3. Calculated molar volume values for three representative compositions.

Au:Fe at %	V/ cm^3/mol
Au	10.21
$Au_{85}Fe_{15}$	9.96
$Au_{50}Fe_{50}$	8.55
$Au_{15}Fe_{85}$	7.4
Fe	6.93

With V_{Au} and V_{Fe} being the molar volume of pure iron and gold, respectively.

2. Model for calculation of the Gibbs free energy for CS NPs (G_{CS})

$$\mathbf{G_{CS} = X_{Au}G_{Au} + X_{Fe}G_{Fe} + \alpha_{Au}S_{Au}\,\gamma_{Au} + \alpha_{Fe}S_{Fe}\,\gamma_{Fe} + G_{int}} \qquad \textit{(eq. S3)}$$

with

$\mathbf{X_{Fe}}$, $\mathbf{X_{Au}}$: the mole fraction of Au and Fe respectively

$\mathbf{G_{Au}}$, $\mathbf{G_{Fe}}$: the molar free energies of pure Au (G_{Au} = -14.1kJ/mol) and Fe (G_{Fe} = -7.95 kJ/mol)[15]

$\boldsymbol{\alpha_{Au}}$, $\boldsymbol{\alpha_{Fe}}$: the fractions of surface atoms of Au and Fe vs the total number of Au and Fe atoms in the particle, where

$\boldsymbol{\alpha_{Fe}} = N_{Fe}/n_{Fe}$

$\boldsymbol{\alpha_{Au}} = N_{Au}/n_{Au}$

with

$\mathbf{n_{Au}}$, $\mathbf{n_{Fe}}$: total number of Au or Fe atoms, that for a core-shell is given by

$\mathbf{n_{Fe}} = R_{Fe}^3/r_{Fe}^3 f_{Fe}$

$\mathbf{n_{Au}} = R_{Au}^3/r_{Au}^3 f_{Au} - R_{Fe}^3/r_{Au}^3 f_{Au}$

with

$\mathbf{f_{Au}}$, $\mathbf{f_{Fe}}$: the packing fraction for Au and Fe structures. 0.74 was used for fcc structure and applied for Au and 0.68 was used for bcc structure applicable to Fe

$\mathbf{r_{Au}}$, $\mathbf{r_{Fe}}$: the atomic radii of the Au or Fe structure

$\mathbf{r_{Au}}$: 0.288 nm (for fcc structure)[21]

$\mathbf{r_{Fe}}$: 0.248 nm (for bcc structure)[18]

$\mathbf{N_{Au}}$, $\mathbf{N_{Fe}}$: number of the surface atoms of Au or Fe, given by

$\mathbf{N_{Fe}} = \pi\alpha f_{Fe}^{-2/3} n_{Fe}^{2/3}$

$\mathbf{N_{Au}} = \pi\alpha f_{Au}^{-2/3} n_{Au}^{2/3}$

with

$\boldsymbol{\alpha}$: the shape factor (defined as the surface area ratio of non-spherical and spherical nanoparticles of identical volumes); $\alpha = 1$ for spherical nanoparticles[19]

$\mathbf{R_{Au/Fe}}$: the radius of the iron core for Fe, or the radius of the whole particle for Au, as illustrated in the following Figure S7.

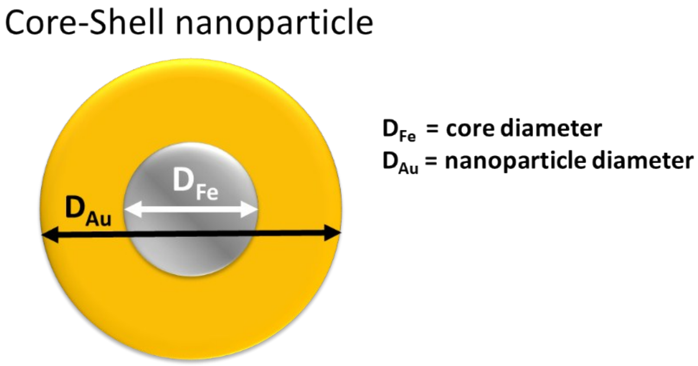

Figure S8. Schematic representation illustrating how core and shell diameters are identified.

The diameter of the iron core was calculated based on simple geometric assumptions. The following Table S4 depicts the Fe-core diameters in correlation with particle composition and overall particle diameter:

Table S4. Atomic versus Volume fraction in CS NPs.

Atomic versus Volume fractions in CS NPs with different Fe content	
atomic %	**Vol %**
85	80
50	41
15	11

$\mathbf{S_{Au}}$, $\mathbf{S_{Fe}}$: the surface areas occupied by 1 mole of atoms of Au and Fe, respectively, where

$\mathbf{S_{Au}} = 4.3 \times 10^4\ m^2$

$\mathbf{S_{Fe}} = 3.2 \times 10^4\ m^2$

$\boldsymbol{\gamma_{Au}}, \boldsymbol{\gamma_{Fe}}$: the size dependent specific surface energy (surface energy per unit area) of the nanoparticle for either Au and Fe atoms, given by:

$\boldsymbol{\gamma_{Fe}} = N_{Fe}\, E_s(D_{Fe}) / \pi\alpha N_A D_{Fe}^2\ [Jm^{-2}]$ *(eq. S4a)*

$\boldsymbol{\gamma_{Au}} = N_{Au}\, E_s(D_{Au}) / \pi\alpha N_A D_{Au}^2\ [Jm^{-2}]$ *(eq. S4b)*

with

$\mathbf{N_{Au}}$, $\mathbf{N_{Fe}}$: the number of atoms on the surface of a particle of diameter $\mathbf{D_{Au}}$, $\mathbf{D_{Fe}}$ (for $\boldsymbol{\gamma_{Au}}$ the particle surface is equal to the surface of the NPs (Au is outside), while for $\boldsymbol{\gamma_{Fe}}$ the surface of the iron core is assumed, Figure S8).

$\mathbf{N_{Au/Fe}} = \pi\alpha f_{Au/Fe}^{-2/3} n_{Au/Fe}^{2/3}$

with

α : the shape factor (defined as the surface area ratio of non-spherical and spherical nanoparticles of identical volumes) α= 1 for spherical nanoparticles[19]

$\mathbf{f_{Au}}$, $\mathbf{f_{Fe}}$: the packing fraction for different structures. 0.74 was used for FCC structure and applied for Au and 0.68 was used for BCC structure applicable to Fe

$\mathbf{n_{Au/Fe} = R_{Au/Fe}^3 / r_{Au/Fe}^3 f_{Au/Fe}}$

with

$\mathbf{r_{Au}}$, $\mathbf{r_{Fe}}$: the atomic radii of Au and Fe in the respective structures

$\mathbf{r_{Au}}$: 0.288 nm (for fcc structure)

$\mathbf{r_{Fe}}$: 0.248 nm (for bcc structure)

$\mathbf{R_{Au}}$, $\mathbf{R_{Fe}}$: the radii of spherical nanocrystal; for Fe we assumed the radius of the iron core, while for Au we assumed the diameter of the whole particle as illustrated in Figure S8.

$\mathbf{E_s(D_{Au})}$, $\mathbf{E_s(D_{Fe})}$: size-dependent specific surface energy for a particle of size $\mathbf{D_{Au}}$ or $\mathbf{D_{Fe}}$

For each metal (Au or Fe):

$\mathbf{E_s(D)} = \{2-[Z_s(D)/Z_b] - [Z_s(D)/Z_b]^{1/2}\} E_{ci}(D)/2$

$\mathbf{E_{ci}(D)} = E_c(D)/\{1-p(D)\{2-[Z_s[D]/Z_b] - -[Z_s[D]/Z_b]^{1/2}\}/2$

$\mathbf{p(D)} = N_s(D)/N_{tot}(D)$

where:

$\mathbf{Z_s(D)}$: size dependent average surface coordination number of the metal

$\mathbf{Z_b}$: the average coordination number of the internal atoms of the metal

$\mathbf{E_c(D)}$: size and composition dependent cohesive energy for that metal

$\mathbf{E_c(D_{Au})} = E_{Au}\, (1-(\alpha D_{Au}2/nd_{Au}^2)$

$\mathbf{E_c(D_{Fe})} = E_{Fe}\, (1-(\alpha D_{Fe}2/nd_{Fe}^2)$

with

$\mathbf{E_{Au}}$, $\mathbf{E_{Fe}}$: the bulk cohesive energies of Au and Fe, respectively.

$\mathbf{E_{Au}}$: 368 kJ/mol

$\mathbf{E_{Fe}}$: 413 kJ/mol

$\mathbf{D_{Au}}$, $\mathbf{D_{Fe}}$: the radii of spherical nanocrystal; for Fe we assumed the radius of the iron core, while for Au we assumed the diameter of the whole particle as illustrated in Figure S8.

$\mathbf{d_{Au}}$, $\mathbf{d_{Fe}}$: are the atomic diameters of Au and Fe, respectively.

N : total number of atoms in the particle

p(D) : is the relation between the total number of atoms present on the surface $\mathbf{N_s(D)}$ and inside a particle $\mathbf{N_{tot}(D)}$ of a given size, respectively

$\boldsymbol{\alpha}$: the shape factor (defined as the surface area ratio of non-spherical and spherical nanoparticles of identical volumes); $\alpha = 1$ for spherical nanoparticles

$\mathbf{G_{int}}$: the Gibbs free energy contribution given by the geometrical ($\gamma_{\mathbf{geo}}$) and chemical ($\gamma_{\mathbf{chem}}$) factors, that can be written as:

$\mathbf{G_{int}} = A\,(\gamma_{geo} + \gamma_{chem})$ *(eq. S5)*

$\gamma_{\mathbf{geo}} = (F/2)\,(\gamma_{Au} + \gamma_{Fe})$ *(eq. S5a)*

$\gamma_{\mathbf{chem}} = \{X_{Au}\,\Delta H_{Au\_in\_Fe} / [C_o(V_{Au})^{2/3} + X_{Fe}\,\Delta H_{Fe\_in\_Au} / [C_o(V_{Fe})^{2/3}]\}$ *(eq. S5b)*

Resulting in:

$\mathbf{G_{int} = A\,[(0.33/2)\,(\gamma_{Au} + \gamma_{Fe})] + [\{X_{Au}\,\Delta H_{Au\_in\_Fe} / [C_o(V_{Au})^{2/3} + X_{Fe}\,\Delta H_{Fe\_in\_Au} / [C_o(V_{Fe})^{2/3}]\}]}$ *(eq. S6)*

with

A : surface area occupied by 1 mole of interfacial atoms, as described in Table S5 below

Table S5. Calculated values for surface area occupied by 1 mole of interfacial atoms

Au:Fe at %	**A / m^2**
Au	4.3 x10^4
$Au_{85}Fe_{15}$	4.13 x 10^4
$Au_{50}Fe_{50}$	3,79 x 10^4
$Au_{15}Fe_{85}$	3.36 x 10^4
Fe	3.2 x 10^4

F = 0.33 : The multiplication factor of 0.33 is based on the assumption that the grain boundary energy is 30 % of the surface energy at 0 K[13]

$\mathbf{\Delta H_{Au\_in\_Fe}}$, $\mathbf{\Delta H_{Fe\_in\_Au}}$: the heat of solution of Au in Fe (or Fe in Au) at infinite dilution, according to ref.[13];

$\gamma_{\mathbf{Au}}$, $\gamma_{\mathbf{Fe}}$ are calculated based on *eq. S4* and are summarized in Table S6

Table S6. Calculated values for size dependent surface energies for $Au_{50}Fe_{50}$

NPs size (nm)	γ_{Au} **(Jm^{-2})**	γ_{Fe} **(Jm^{-2})**
5	0.00173	0.00221
7.5	0.00164	0.00211
10	0.0016	0.00208
15	0.00157	0.00205
20	0.00155	0.00204
25	0.00154	0.00203
30	0.00154	0.00203
35	0.00153	0.00202
40	0.00153	0.00202
45	0.00153	0.00202
50	0.00153	0.00202

$\mathbf{X_{Au}}$, $\mathbf{X_{Fe}}$: are the molar fraction of Au and Fe, respectively

$\mathbf{\Delta H}$: is the heat of solution of Au in Fe (or Fe in Au) at infinite dilution, where[19]

$\Delta H_{Au\_in\_Fe} = 8$ kJ/mol

$\Delta H_{Fe\_in\_Au} = 6$ kJ/mol

$\mathbf{C_0}$: is a constant being 4.5×10^8.

V : are the molar volumes of Au and Fe, respectively, where[22]

$V_{Au} = 10.21$ cm^3/mol for Au fcc

$V_{Fe} = 7.09$ cm^3/mol for Fe bcc

An example of Gibbs free energy for three representative compositions of Fe-Au CS NPs is reported in the previous Figure S7.

References.

1 E. Cattaruzza, G. Battaglin, F. Gonella, R. Polloni, B. F. Scremin, G. Mattei, P. Mazzoldi and C. Sada, *Appl. Surf. Sci.*, 2007, **254**, 1017–1021.

2 E. Cattaruzza, G. Battaglin, P. Riello, D. Cristofori and M. Tamisari, *Appl. Surf. Sci.*, 2014, **320**, 863–870.

3 V. Amendola, S. Scaramuzza, F. Carraro and E. Cattaruzza, *J. Colloid Interface Sci.*, 2017, **489**, 18–27.

4 E. C. Le Ru and P. G. Etchegoin, *Chem. Phys. Lett.*, 2006, **423**, 63–66.

5 V. Amendola, S. Scaramuzza, S. Agnoli, S. Polizzi and M. Meneghetti, *Nanoscale*, 2014, **6**, 1423–

1433.

6 V. Amendola, R. Pilot, M. Frasconi, O. M. Maragò and M. A. Iatì, *J. Phys. Condens. Matter*, 2017, 29, 203002.

7 B. T. Draine and P. J. Flatau, *arXiv*, 2010, 1002.1505.

8 B. T. Draine and P. J. Flatau, *J.Opt.Soc.Am.A*, 1994, **11**, 1491–1499.

9 J. J. Goodman, B. T. Draine and P. J. Flatau, *Opt.Lett*, 1991, **16**, 1198–1200.

10 R. L. Olmon, B. Slovick, T. W. Johnson, D. Shelton, S.-H. Oh, G. D. Boreman and M. B. Raschke, *Phys. Rev. B*, 2012, **86**, 235147.

11 P. Johnson and R. Christy, *Phys. Rev. B*, 1974, **9**, 5056–5070.

12 U. Kreibig and M. Vollmer, *Optical Properties of Metal Clusters*, Springer, Berlin, 1995.

13 C. Srivastava, S. Chithra, K. D. Malviya, S. K. Sinha and K. Chattopadhyay, *Acta Mater.*, 2011, **59**, 6501–6509.

14 W. T. Osowiecki, X. Ye, P. Satish, K. C. Bustillo, E. L. Clark and A. P. Alivisatos, *J. Am. Chem. Soc.*, 2018, **140**, 8569–8577.

15 I. Barin, O. Knacke and O. Kubaschewski, *Thermochemical properties of inorganic substances*, Springer Berlin Heidelberg, Berlin, Heidelberg, 1977.

16 H. Okamoto, T. B. Massalski, L. J. Swartzendruber and P. A. Beck, *Bull. Alloy Phase Diagrams*, 1984, **5**, 592–601.

17 W. Mönch, *Semiconductor Surfaces and Interfaces*, Springer Berlin Heidelberg, Berlin, Heidelberg, 2001, vol. 26.

18 H. Fredriksson, U. Akerlind and Wiley InterScience (Online service), *Physics of functional materials*, John Wiley & Sons, 2008.

19 W. H. Qi, M. P. Wang, M. Zhou and W. Y. Hu, *J. Phys. D. Appl. Phys.*, 2005, **38**, 1429–1436.

20 C. Kittel, *Introduction to solid state physics*, Wiley, 2005.

21 R. H. Williams, *Semiconductor surfaces and interfaces*, Springer Science & Business Media, 1983, vol. 33.

22 C. N. Singman, *J. Chem. Educ.*, 1984, **61**, 137.